Geochemistry Geophysics Geosystems G3
AN ELECTRONIC JOURNAL OF THE EARTH SCIENCES
Published by AGU and the Geochemical Society

Article
Volume 8, Number 5
26 May 2007
Q05012, doi:10.1029/2006GC001532
ISSN: 1525-2027

Variations of the ACC-CDW during MIS3 traced by magnetic grain deposition in midlatitude South Indian Ocean cores: Connections with the northern hemisphere and with central Antarctica

A. Mazaud, C. Kissel, C. Laj, M. A. Sicre, and E. Michel
Laboratoire des Sciences du Climat et de l'Environnement, CEA-CNRS, Domaine du CNRS, F-91198 Gif-sur-Yvette, France (mazaud@lsce.cnrs-gif.fr)

J. L. Turon
Département de Géologie et Océanographie, UMR#505, Université Bordeaux I, Avenue des Facultés, F-33405, Talence Cedex, France

[1] We examine the magnetic mineral deposition in three cores located at midlatitude sites in the South Indian Ocean, in an area where sediment eroded from the Kerguelen-Crozet plateau and transported by the marine currents, principally the Antarctic Circum Current, accumulates at a high sedimentation rate. We focus on Marine Isotopic Stage 3, characterized by large climatic fluctuations at northern latitudes, and compare the obtained records to the climatic records at Byrd (Antarctica) and Summit (GISP2, Greenland) and to the North Atlantic Deep Water variations in the North Atlantic. Magnetic mineral deposition at the studied sites exhibits a profile with maxima at the time of Heinrich events H4 and H5, which suggests a strong Antarctic Circum Current when the North Atlantic Deep Water was reduced at northern latitude during these events. We show that an interhemispheric seesaw, characterized by temporary surface warmings in the southern hemisphere, is also marked by a strong Antarctic Circum Current at the time of the northern Heinrich events. The rapid Dansgaard-Oeschger oscillations evidenced in the northern records after interstadials IS12 and IS8 are not visible, suggesting a limited counterpart of these events in the midlatitude southern Indian Ocean.

Components: 4603 words, 11 figures, 1 table.

Keywords: paleoceanography; south; Indian; ocean.

Index Terms: 0473 Biogeosciences: Paleoclimatology and paleoceanography (3344, 4900); 1512 Geomagnetism and Paleomagnetism: Environmental magnetism; 4938 Paleoceanography: Interhemispheric phasing.

Received 17 November 2006; **Revised** 8 February 2007; **Accepted** 21 February 2007; **Published** 26 May 2007.

Mazaud, A., C. Kissel, C. Laj, M. A. Sicre, E. Michel, and J. L. Turon (2007), Variations of the ACC-CDW during MIS3 traced by magnetic grain deposition in midlatitude South Indian Ocean cores: Connections with the northern hemisphere and with central Antarctica, *Geochem. Geophys. Geosyst.*, *8*, Q05012, doi:10.1029/2006GC001532.

1. Introduction

[2] The last glacial period is characterized by different climatic variations in the two hemispheres. In the north, Heinrich (H) and Dansgaard-Oeschger (DO) events are associated to large temperature oscillations over the central Greenland [*Dansgaard et al.*, 1993; *Bond and Lotti*, 1995; *Grootes and Stuiver*, 1997]. Concomitant changes in the North Atlantic Deep Water (NADW) current were documented by magnetic mineral deposition in several cores located along the NADW path [*Kissel et al.*, 1999; *Laj et al.*, 2002; *Ballini et al.*, 2006]. Central Antarctic ice reveals a somewhat different pattern, with less abrupt variations. Progressive warmings, called the "A" events, started ≈1.5 kyr before the interstadials (IS) in the north hemisphere, according to the pole-to-pole synchronization derived from ice-trapped atmospheric methane [*Blunier and Brook*, 2001]. A seesaw mechanism was advocated, in which the southern hemisphere warms when the northern hemisphere cools [*Broecker*, 1998; *Stocker*, 1998, 2002; *Stocker and Johnsen*, 2003]. New data from the southeast Pacific suggest that the seesaw has also operated in the past 350 kyr [*Pahnke and Zahn*, 2005]. However, the interconnection between the climatic fluctuations in the two hemispheres, and in particular the role of the southern ocean in heat storage and transport, are not known in detail. Here, we focus on the southern ocean, in a zone where the eastward flow of the Antarctic Circumpolar Current (ACC) transports a substantial fraction of the NADW from the Atlantic to the other oceans [*Rintoul et al.*, 2001]. We attempt to decipher the millennial scale variations of the ACC in the south Indian Ocean during marine isotopic stage (MIS) 3, characterized by large and rapid climatic fluctuations at northern latitudes. We examine past changes in the magnetic mineral content of three marine cores located at mid latitude eastward of the volcanic Kerguelen and Crozet plateau, in an area where previous studies evidenced a large accumulation of sediment, principally issued from the Kerguelen and Crozet plateau and transported to the sites by the Antarctic Circumpolar Current – Circumpolar Deep Water (ACC-CDW) [*Bareille et al.*, 1994; *Dezileau et al.*, 2000] (Figure 1b). The obtained records are placed on the GISP2 chronology and compared to climate change over Greenland and Antarctica, and to the strength of the NADW, as documented by magnetic material content of several cores along the NADW path [*Kissel et al.*, 1999; *Laj et al.*, 2002; *Ballini et al.*, 2006].

2. Marine Core Locations and Oceanographic Context

[3] The studied marine cores were taken at mid latitude in the South Indian Ocean, eastward of the Kerguelen plateau. They are located at ≈45° south near the southern flank of the South Indian Ocean ridge (Figures 1 and 2). In this area, detrital materials issued from the Crozet-Kerguelen plateau accumulated at a high deposition rate in an oblong sedimentary tongue (Figure 2). Cores MD94-103 and MD94-104 were taken at depth of ≈3500 m during the PACIMA cruise of the Research Vessel *Marion Dufresne* of the French Polar Institute (IPEV). Core MD88-769 was obtained in the same sedimentary formation, but at a more distant position from the Kerguelen plateau than the two other cores (Figure 2). Core locations core lengths and water depths are given in Table 1.

[4] Previous isotopic studies allowed the identification of the Marine Isotopic Stage (MIS) 1 to 6. Low-resolution records of low field magnetic susceptibility (κ) revealed a higher magnetic susceptibility during MIS 2 and 4 than during MIS 5 and the Holocene [*Dezileau et al.*, 2000]. Enhanced input of magnetic material during cold MIS was attributed to a more efficient erosion and transport by the ACC of material issued from the Kerguelen and Crozet plateau during MIS 2 and 4 than during Holocene, MIS3 and MIS5, with lateral redistribution [*Dezileau et al.*, 2000]. The Antarctic Bottom Water (AABW) current also flows in this zone, at a depth of ≈4000 m at present time. Analyses of rare earths indicated that only minor amount of particles issued from Antarctica reached the studied formation during the last glacial epoch [*Dezileau et al.*, 2000].

3. Magnetic Investigations

[5] Magnetic analyses consist of continuous high-resolution measurements of the bulk magnetic parameters used to characterize the nature and the amount of the magnetic fraction deposited in the sediment. Bulk magnetic parameters are the volume low-field susceptibility (κ), the Anhysteretic Remanent Magnetization (ARM), and the Isothermal Remanent Magnetization (IRM). κ reflects the amount, nature and grain size of ferromagnetic (*s.l.*) and paramagnetic minerals. ARM and IRM,

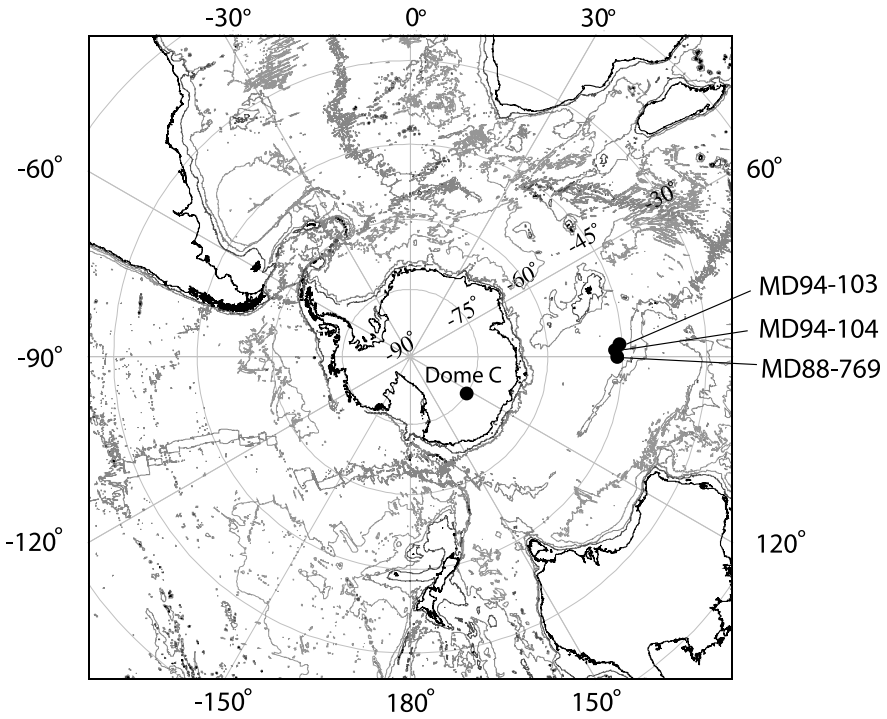

Figure 1. Global map of the southern Indian Ocean showing the location of the studied cores. Location of Dome C in Antarctica is also indicated.

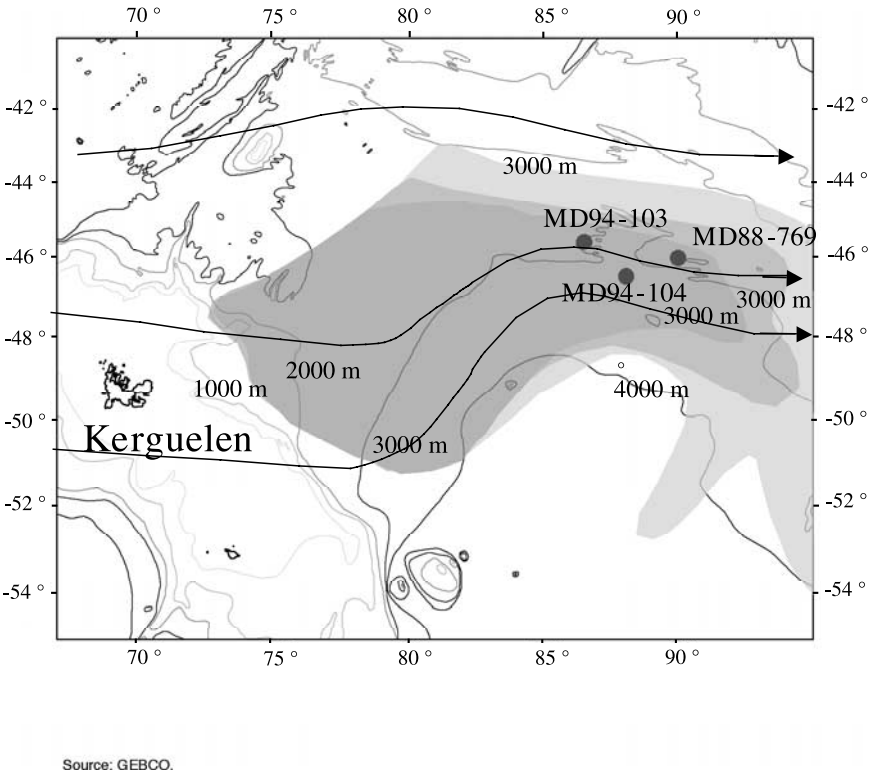

Figure 2. Site locations marine and topography. Grayed areas indicate estimates of the sediment thickness, after *Dezileau et al.* [2000] (dark: > 500 m, mid: 250 ≪ 500 m, light: < 250 m). The ACC flow is schematically indicated by the arrows.

Table 1. Location and Water Depths of the Studied Cores

Core Name	Longitude, E	Latitude, S	Water Depth, m
MD94-103	86°32	45°35	3559
MD94-104	88°04	46°29	3460
MD88-769	90°06	46°04	3420

on the other hand, are remanent magnetizations, and therefore are solely sensitive to the ferro/ferri magnetic fraction, and do not depend on paramagnetic minerals. ARM is principally linked to small magnetic grains, with size around 0.1 – 5 mumeter, while IRM is sensitive to a wider spectrum of grain size [*Verosub and Roberts*, 1995]. ARM and IRM were measured after full demagnetization of the Natural Remanent Magnetization (NRM). To measure NRM, κ, ARM, and IRM, the cores have been continuously subsampled using the u-channel technique [*Tauxe et al.*, 1983; *Weeks et al.*, 1993].

[6] κ, previously measured at a 12.5 cm resolution, was remeasured at the LSCE using a small diameter Bartington coil, allowing a resolution of 4 cm, very close to that of the cryogenic magnetometers used for ARM and IRM determinations. NRM, ARM and IRM records were obtained in the shielded room of the LSCE with high-resolution

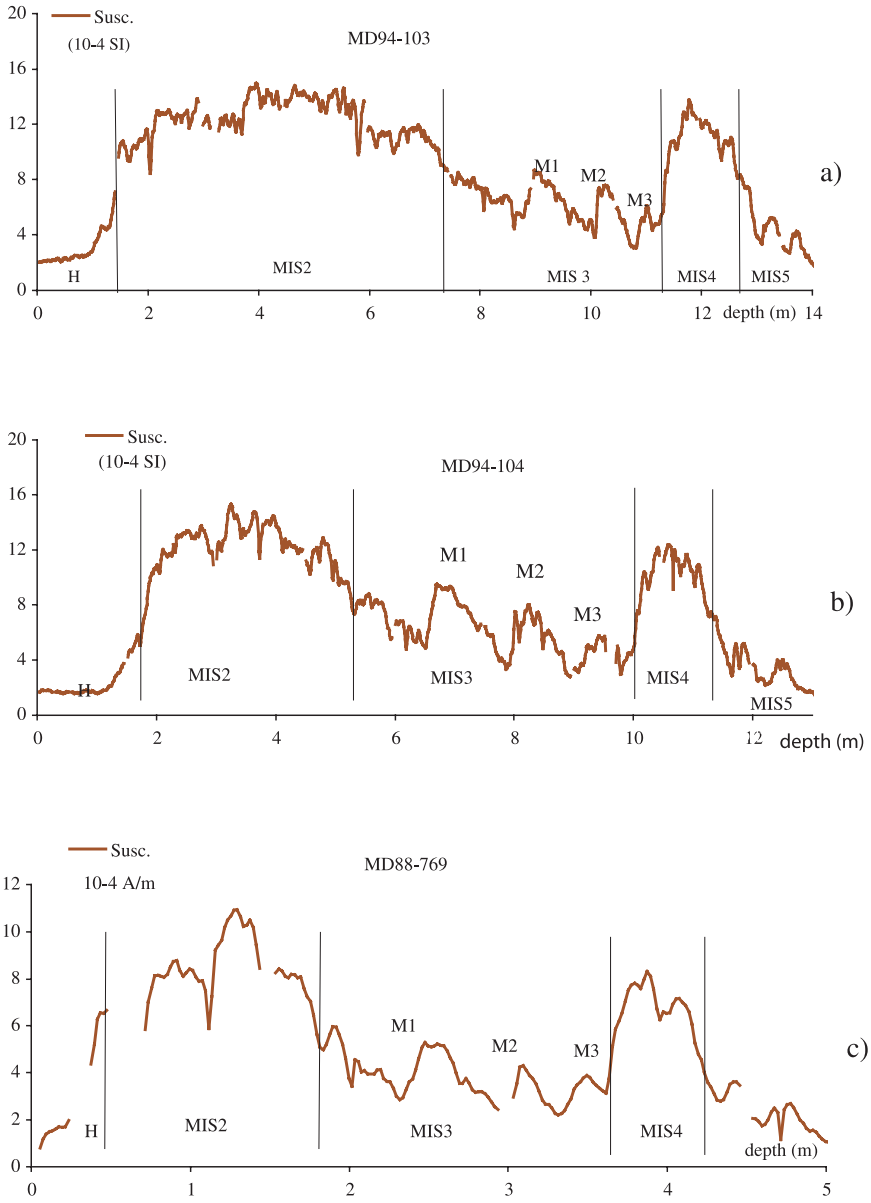

Figure 3. Low field susceptibility (κ) measured at high resolution for the 3 cores: (a) MD94-103, (b) MD94-104, and (c) MD88-769. Positions of the Marine Isotopic Stages as identified by *Dezileau et al.* [2000] are also indicated.

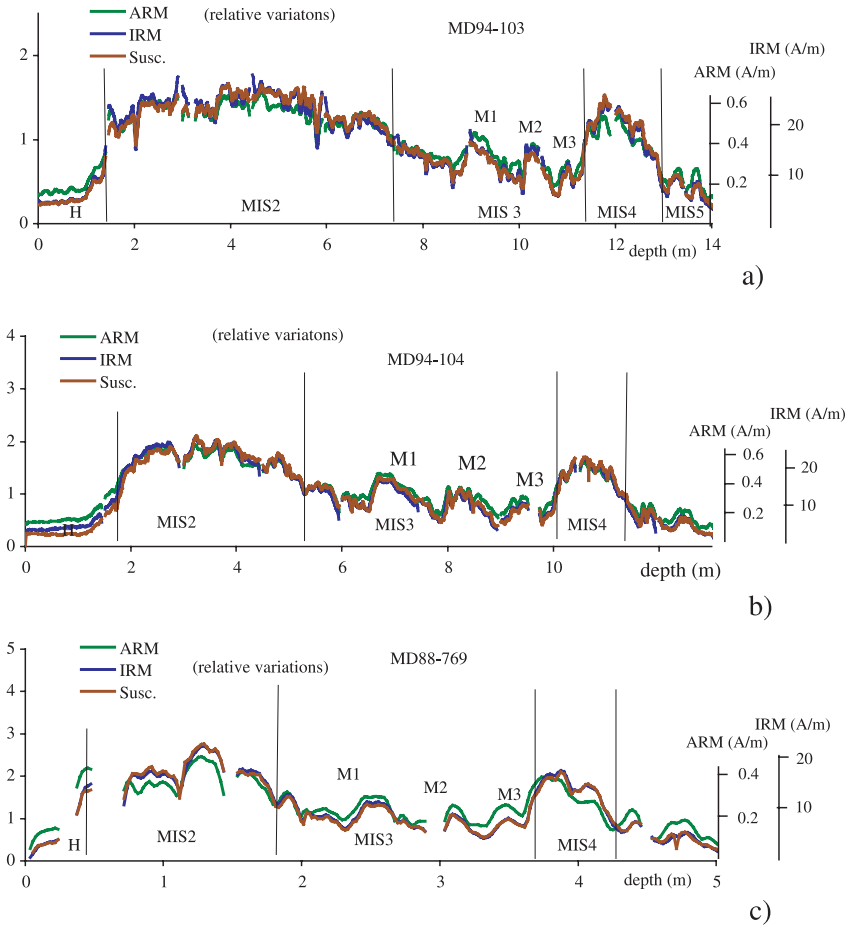

Figure 4. Variations of the low field susceptibility (κ), ARM, and IRM obtained for the 3 cores: (a) MD94-103, (b) MD94-104, and (c) MD88-769.

pass-through 2G cryogenic magnetometers [*Goree and Fuller*, 1976; *Weeks et al.*, 1993]. ARM was imparted along the axis of the u-channel in a 100 mT AF and 0.05 mT bias field, followed by ARM AF demagnetization with 8 steps from 0 to 70 mT. IRM was then acquired in 6 steps up to 1T using a 2G pulsed IRM solenoid.

[7] Records of κ obtained at the three sites exhibit similar patterns, and MIS boundaries already identified by *Dezileau et al.* [2000] are easily identifiable (Figure 3). During MIS3, 3 peaks labeled M1, M2 and M3 are visible in the ARM, IRM and κ records, which document similar variations (Figure 4). This similarity indicates that the bulk parameters, ARM, IRM and κ, principally trace the concentration of the ferro/ferri magnetic grains, with limited changes in magnetic mineralogy and grain size, because such changes would have affected differently ARM, IRM and κ. General homogeneity of the magnetic content of these sediments is indicated by the small dispersion of the points along a straight line in an ARM versus κ diagram (Figure 5). Thermomagnetic analyses conducted on core MD94-103 indicate magnetite or low Ti-content (titano)-magnetite and hysteresis experiments document grain size in the pseudo-single domain (PSD) range (i.e., grains of a few microns) [*Mazaud et al.*, 2002]. ARM/IRM, a

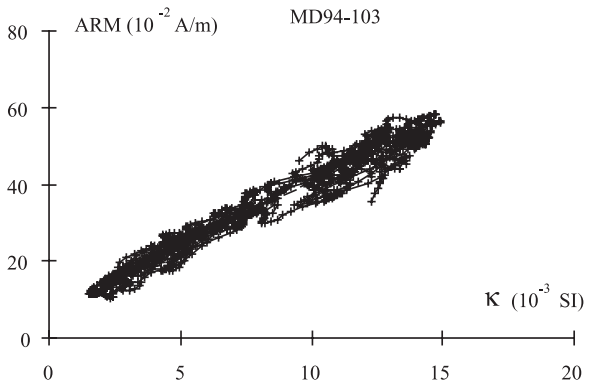

Figure 5. ARM plotted against κ.

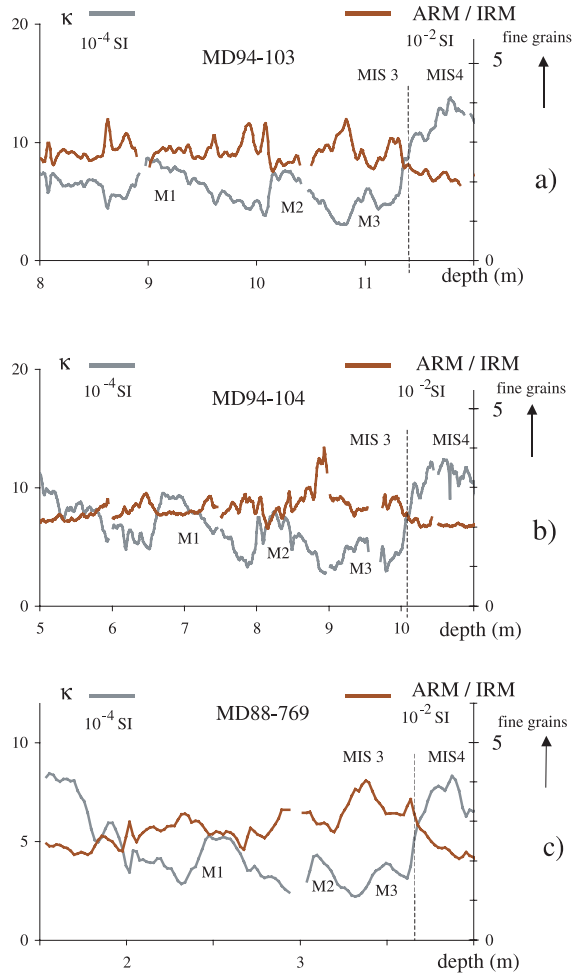

Figure 6. Variations of ARM/IRM and κ obtained for three cores: (a) MD94-103, (b) MD94-104, and (c) MD88-769.

proxy for magnetite grain size variations [*Verosub and Roberts*, 1995], exhibits limited changes, as expected from the resemblance of ARM, IRM and κ. Largest values (smallest grains) are obtained after M1, M2, and M3, when ARM, IRM and κ indicate low concentration (Figure 6). The question is now to determine how these bulk magnetic parameters trace past changes in the flux of the magnetic minerals, and how they are connected to the concomitant climatic fluctuations.

4. Age Model

[8] The 3 studied cores are placed on a common chronology, GISP2 [*Grootes and Stuiver*, 1997]. The age model for the upper part of the core was derived from ^{14}C AMS dating [see *Sicre et al.*, 2005, Table I]. In the 30–50 kyr B.P. interval, the age model of core MD94-103 was previously derived from a geomagnetic correlation of its paleointensity signal to the NAPIS-75 stack [*Mazaud et al.*, 2002]. Figure 7a shows the match between MD94-103 and NAPIS-75, and Figure 7b shows the derived age model and the corresponding sedimentation rate. Best correlation was obtained in the 30–45 kyr B.P. interval, where sedimentation rate approximates 20 cm/kyr (Figure 7b), while the correlation for ages older than 45 kyr is less precise (Figure 7a). The target paleointensity stack, NAPIS-75, was obtained from North Atlantic cores and placed on the GISP2 chronology [*Laj et al.*, 2000]. A drop in intensity coincident to a directional excursion is observed in core MD94-103 within MIS3. It was associated to the Laschamp geomagnetic event, dated in NAPIS-75 at ≈41 kyr. Best correlation to NAPIS-75 was obtained in the 30–45 kyr B.P., with uncertainties of ≈500 years or less [*Mazaud et al.*, 2002]. No precise chronology was obtained for ages older than 50 kyr B.P. and for ages younger than 30 kyr B.P., estimated by interpolating available radiocarbon ages [*Sicre et al.*, 2005].

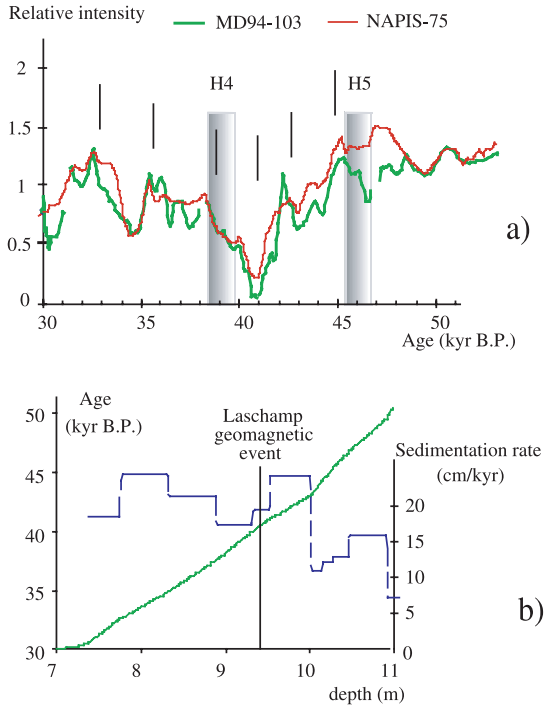

Figure 7. (a) Correlation of core MD94-103 geomagnetic intensity record to the NAPIS-75 stack (figure from *Mazaud et al.* [2002]). The tie points are indicated by vertical lines. The Laschamp geomagnetic event corresponds to the geomagnetic intensity low at ≈41 kyr B.P. (b) Age model of core MD94-103 and derived accumulation rate.

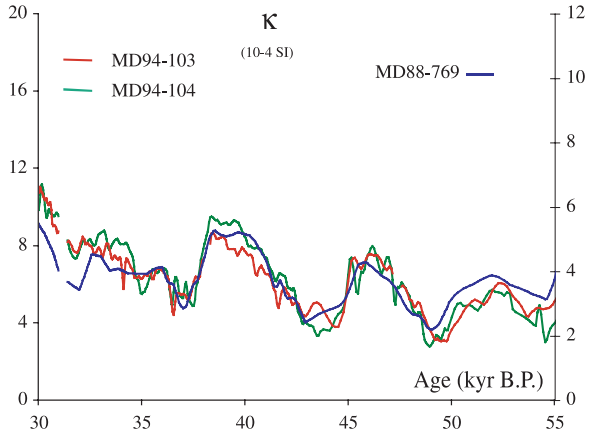

Figure 8. The susceptibility records obtained for the 3 cores during MIS3 after correlating cores MD94-104 and MD88-769 to core MD94-103.

[9] The two other cores, MD94-104 and MD88-769, were placed on the same chronology by correlating their bulk susceptibility to that of core MD94-103 (Figure 8). This approach, however, is based on the hypothesis that the bulk magnetic parameters have varied simultaneously at the three sites, so that they can be used to synchronize the 3 cores. To test a posteriori this hypothesis, we have examined the paleointensity profiles obtained for the three cores by normalizing their Natural Remanent Magnetization (NRM) intensity by the ARM. On the basis of the correlation of the susceptibility records, the paleointensity drops associated to the Laschamp geomagnetic event coincide (Figure 9). This coincidence is a good indication that the variations in κ, ARM, or IRM, were synchronous at the 3 sites, so that they can be used for regional correlations around the Laschamp geomagnetic event.

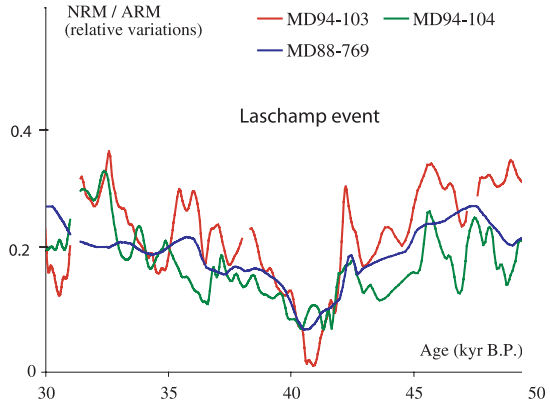

Figure 9. Relative paleointensity records obtained after correlating the susceptibility records of cores MD94-104 and MD88-769 to that of core MD94-103.

5. Magnetic Grain Deposition in the 30–50 kyr B.P. Interval

[10] Variations in concentration of (titano)magnetite grains may be caused by changes in the flux of the magnetite, and/or by changes in the flux of nonmagnetic, or low-magnetic constituents, which dilute the magnetic phase in the sediment. To test whether or not the observed variations trace past changes in the deposition rate of magnetic grains, we have calculated for core MD94-103 a susceptibility profile in which the dilution by the calcium carbonate content (Figure 10) was removed. The

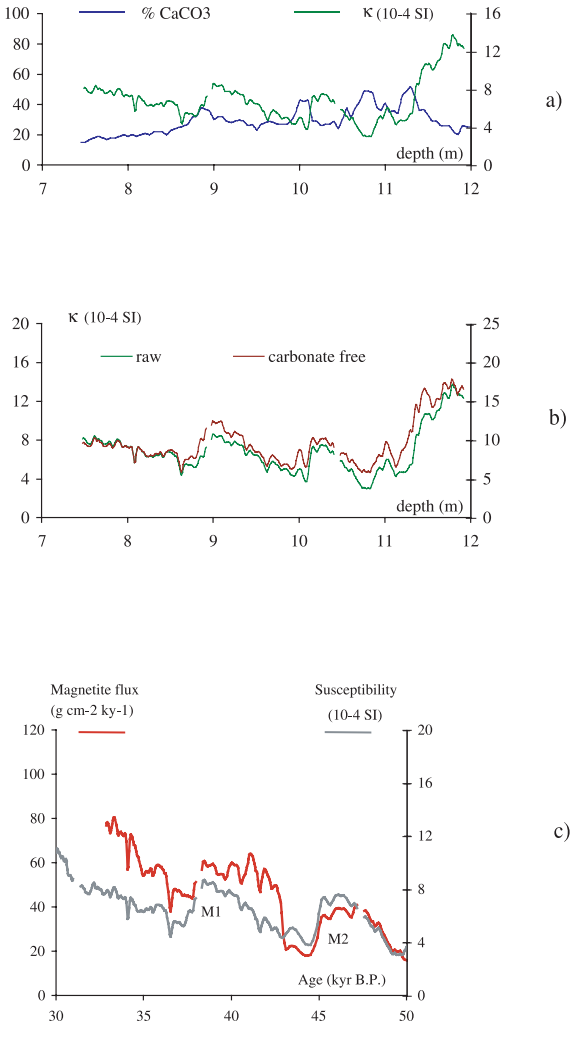

Figure 10. (a) Percentage of $CaCO_3$ in core MD94-103, (b) low field susceptibility before and after carbonate detrending, and (c) magnetite flux calculated for core MD94-103 in the 30–50 kyr B.P. interval.

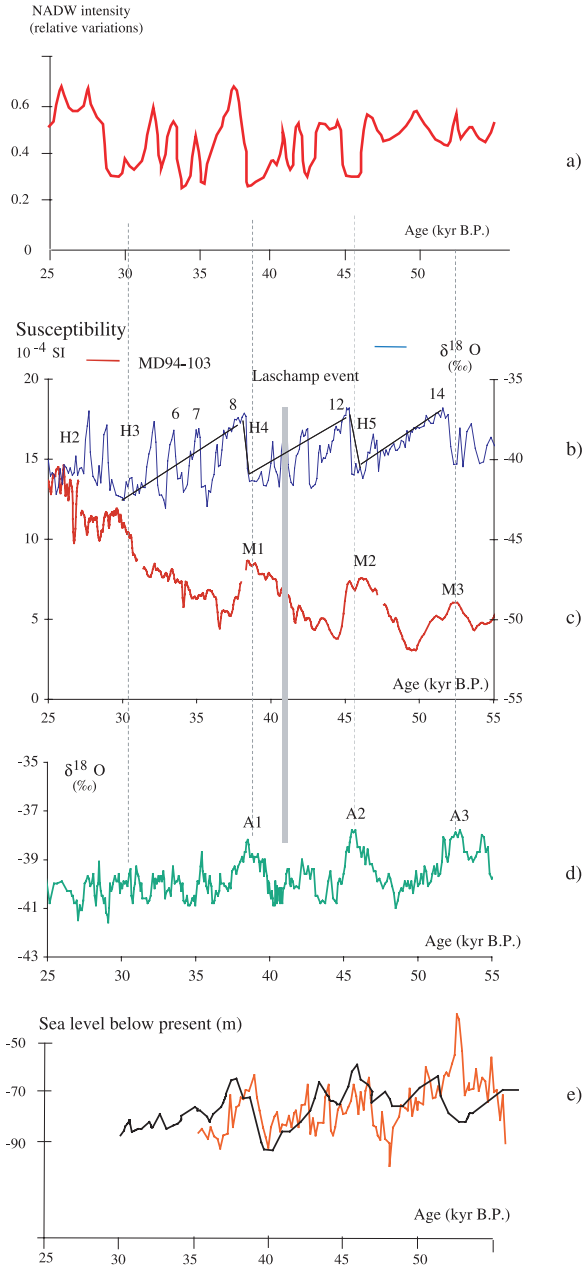

Figure 11. (a) Past variations in the 30–50 kyr B.P. of the NADW (figure after *Laj et al.* [2002]), (b) GISP2 isotopic record [*Grootes and Stuiver*, 1997], (c) magnetic mineral concentration eastward of the Kerguelen plateau, (d) Byrd isotopic record, and (e) the sea level (orange curve: *Siddal et al.* [2003]; dark curve: *Arz et al.* [2006]). All records are placed on the GISP2 age model. The "Bond" cycles are indicated by the gray lines in the GISP2 isotopic record [see also *Bond et al.*, 1993].

magnetic deposition "M" events are still clearly seen in this "carbonate free" record (Figure 10b), so that these events do not correspond to change in the dilution of the magnetic fraction by carbonates. Because other nonmagnetic or low-magnetic materials may have also diluted the ferro/ferri magnetic fraction, we have also attempted to calculate the flux of magnetite arriving in core MD94-103 in the 30–50 kyr B.P. interval, an interval which includes the events M1 and M2 by considering the accumulation rates of core MD94-103 as derived from its age model [*Mazaud et al.*, 2002]. In this simple calculation, it was assumed that the low field susceptibility κ was carried by the magnetite grains. Paramagnetic contribution was neglected because of the high level of κ and of the resemblance between ARM, IRM, and κ records (see also section 3). Influence of grain size variations on κ was neglected, and a specific value of 5 10^{-4} m^3 kg^{-1} for the mass specific susceptibility of magnetite was used. A density of 5.04 g per cc for pure magnetite was considered for deriving massic flux of magnetite [*Thompson and Oldfield*, 1986]. Obtained flux is shown in Figure 10c. The peaks M1 and M2 are clearly visible, although the shape of the M1 peak is modified (Figure 10c). Thus variations in magnetic grain concentration as traced by κ, ARM, and IRM reflect principally changes in the flux of magnetite deposited at the studied sites. No precise flux calculation was possible outside the 30–50 kyr B.P. interval, because the age model is not precise enough. It is likely, however, that the M3 peak was produced by the same causes than the M1 and M2 peaks.

6. Implications for the ACC-CDW During MIS3

[11] The bulk magnetic parameters exhibit similar "saw tooth" profiles at the 3 sites, so that they principally reflect regional variability. Lower concentrations in magnetic grains were obtained at site MD88-769, located at a greater distance from the Kerguelen than the two other cores. This is consistent with a progressive depletion of the ACC current in magnetite grains during the eastward transport from the Crozet-Kerguelen plateau. The modulation of the grain size, with smaller grain size at the time of minimal deposition (Figure 6), suggests a modulation of the intensity of the ACC-CDW current which erodes and conveys the magnetic grains at the sites. It may also reflect variations in material input at the source not necessarily related to ACC-CDW changes. It is likely, however, that such changes would be connected to sea level fluctuations, which may control the input of material at the plateau margin. The sea level curve, as documented by benthic oxygen isotope of core MD95-2042 [*Shackleton et al.*, 2000] and by *Siddal*

et al. [2003] (Figure 11), does not show the "saw tooth" profile seen in magnetic grain deposition. Conversely, a new sea level curve [*Arz et al.*, 2006], documents a sea level drop at the time of H4 and a decrease in the 45–40 kyr B.P interval (Figure 11), suggesting possible correlation between the M1 peak and sea level. Millennial scale changes of sea level are still uncertainly known during MIS3 (Figure 11). However, erosion process at Kerguelen associated to sea level fluctuations may have also contributed to changes in material input at the source. Finally, the "M" peaks could also indicate a change in the position of the ACC-CDW stream, which transports the magnetic grains. However, it is likely that changes in flow trajectory would have affected differently the deposition at 3 different sites, which is not the case. Thus the bulk magnetic and grain size profile reflect alternated periods of reinforcement and weakening of the ACC-CDW current, with a possible contribution of concomitant input changes at the source.

7. Comparison With the Strength of the NADW and With the Greenland and Antarctic Ice Records

[12] The bulk magnetic profile is now compared to the Greenland GISP2 isotopic record [*Grootes and Stuiver*, 1997], the North Atlantic NADW intensity record [*Kissel et al.*, 1999; *Laj et al.*, 2002, *Ballini et al.*, 2006], and the Byrd ice isotopic record from central Antarctica synchronized to the GIPS2 ice [*Blunier and Brook*, 2001]. All the records are here placed on the GISP2 chronology (Figure 11).

[13] The "M1" peak observed in the magnetic grain deposition of the studied cores started during the northern IS 12, and reached a maximum value at the time of H4. Then, a rapid decrease occurred during the northern IS 8. A similar scenario is observed for the "M2" peak, which started at the end of IS14 and reached maximal value during H5. The "M3" peak occurred between IS 15 and IS14, according to the approximate chronology at ages older than 50 kyr B.P. A secondary peak in the magnetic deposition is superimposed to the increasing trend at the time of H3 (Figure 11). No clear modulation corresponds to the rapid Dansgaard-Oeschger oscillations evidenced in Greenland isotopic record and in the NADW record after IS12 and IS 8 (Figure 11).

[14] The "M" maxima also correspond to the "A" events, identified as temporary warmings over the Antarctic at the time of H4, H5 and H6 [*Blunier and Brook*, 2001] (Figure 11). Both "M" and "A" events document a rapid decrease at the onset of IS 8 and 12, after H4 and H5. The Byrd ice isotopic signal, however, does not exhibit a monotonic increase between A1 and A2. Instead, the Byrd ice isotopic record exhibits fluctuations at the millennial scale between H4 and H5, which could be related to the northern D. O. oscillations (Figure 11). Finally, the marked increasing trend after 35 kyr B.P. seen in the bulk magnetic signals of the studied cores is not observed in the Byrd glaciologic signal.

8. Discussion and Conclusion

[15] Magnetic analyses of marine cores taken eastward the Kerguelen plateau indicate enhanced magnetic mineral deposition at the time of H4 and H5, and possibly during the northern stadial before IS14, according to the approximate chronology before 50 kyr B.P. At these epochs, a cold climate and a reduced NADW have existed at northern latitudes. Stable isotopes of core RC11-83, located in the South Atlantic, indicate that NADW input into the South Ocean was also reduced, with a temporary warming of the surface water [*Charles et al.*, 1996; *Ninnemann et al.*, 1999]. Warming over Antarctica is indicated during H4, H5 and H6 by "A" events identified in the Antarctic ice. Foraminifera assemblages at site MD94-103 [*Sicre et al.*, 2005] document rapid fluctuations with some SST increase at the time of H4 and H5 at mid latitude in the south Indian Ocean. Conversely, a rapid decrease in magnetic mineral deposition occurred during the northern interstadials IS12, 14, and 8, when the climate warmed up at high northern latitudes and the NADW restarted after the Heinrich events. This is consistent with an interhemispheric seesaw which has affected both surface temperature and marine currents, with temporary warmings and strong ACC-CDW current in the southern hemisphere at the time of the northern Heinrich events. No modulation of the ACC-CDW corresponds to the northern Dansgaard-Oeschger oscillations. Overall, a global antiphase with the long term cooling cycles identified in the Greenland ice by *Bond et al.* [1993] in particular in the 30–45 kyr B.P. where precise chronology was obtained (Figure 11). Our results therefore suggest that ACC-CDW variations were principally connected to the northern Heinrich events. The northern D.O. oscillations could have been smoothed out by the inertia of the oceanic system. Further studies from

other regions in the southern Ocean are still needed to understand the exact mechanisms involved, in particular the interactions between the different water masses and the atmosphere in the South Ocean.

Acknowledgments

[16] We thank the French institute IPEV, the crew of the R/V *Marion Dufresne* and Yvon Balut, the chief of the operations on the *Marion Dufresne*. Alain Mazaud thanks Claire Waelbroeck for discussions. This study has been funded by the French Commissariat à l'Energie Atomique, by the Centre National de la Recherche Scientifique, and by the European Program Pole-Ocean-Pole EVK2-2000-22067. LSCE contribution 1910.

References

Arz, H. W., F. Lamy, A. Ganopolski, N. Nowaczyk, and J. Pätzold (2006), Dominant Northern Hemisphere climate control over millennial-scale glacial sea-level variability, *Quat. Sci. Rev.*, *26*, 312–321, doi:10.1016/j.quascirev.2006.07.016.

Ballini, M., C. Kissel, C. Colin, and T. Richter (2006), Deep-water mass source and dynamic associated with rapid climatic variations during the last glacial stage in the North Atlantic: A multi-proxy investigation of the detrital fraction of deep-sea sediments, *Geochem. Geophys. Geosyst.*, *7*, Q02N01, doi:10.1029/2005GC001070.

Bareille, G., F. Grousset, M. Labracherie, L. Labeyrie, and J. R. Petit (1994), Origin of detrital fluxes in the southeast Indian Ocean during the last climatic cycles, *Paleoceanography*, *9*, 799–819.

Blunier, T., and E. J. Brook (2001), Timing of millennial-scale climate change in Antarctica and Greenland during the last glacial period, *Science*, *291*, 109–112.

Bond, G., and R. Lotti (1995), Iceberg discharges into the North Atlantic on millennial time scales during the deglaciation, *Science*, *267*, 1005–1010.

Bond, G., W. Broecker, S. Johnsen, J. McManus, L. Labeyrie, J. Jouzel, and G. Bonani (1993), Correlations between climate records from the North Atlantic sediments and Greenland ice, *Nature*, *365*, 143–147.

Broecker, W. S. (1998), Paleocean circulation during the last deglaciation: A bipolar see-saw?, *Paleoceanography*, *13*, 119–121.

Charles, C. D., J. Lynch-Steiglitz, U. S. Ninnemann, and R. G. Fairbanks (1996), Climate connection between the hemispheres revealed by deep sea sediment core/ice correlation, *Earth Planet. Sci. Lett.*, *142*, 19–27.

Dansgaard, W., et al. (1993), Evidence for general instability of past climate from a 250 kyr ice core record, *Nature*, *364*, 218–220.

Dezileau, L., G. Bareille, J. L. Reyss, and F. Lemoine (2000), Evidence for strong sediment redistribution by bottom currents along the southeast Indian Ridge, *Deep Sea Res., Part I*, *47*, 1899–1936.

Goree, W. S., and M. Fuller (1976), Magnetometers using RF-driven squids and their applications in rock magnetism and paleomagnetism, *Rev. Geophys.*, *14*, 591–608.

Grootes, P. M., and M. Stuiver (1997), $^{18}O/^{16}O$ variability in Greenland snow and ice with 10^3 to 10^5 year time resolution, *J. Geophys. Res.*, *102*, 26,455–26,470.

Kissel, C., C. Laj, L. Labeyrie, T. Dokken, A. Voelker, and D. Blamart (1999), Rapid climatic variations during marine isotopic stage 3: Magnetic analysis of sediments from Nordic Seas and North Atlantic, *Earth Planet. Sci. Lett.*, *171*, 489–502.

Laj, C., C. Kissel, A. Mazaud, J. E. T. Channell, and J. Beer (2000), North Atlantic paleointensity stack since 75 ka (NAPIS-75) and the duration of the Laschamp event, *Philos. Trans. R. Soc. London, Ser. A*, *358*, 1009–1025.

Laj, C., C. Kissel, A. Mazaud, E. Michel, R. Muscheler, and J. Beer (2002), Geomagnetic field intensity, North Atlantic Deep Water circulation and atmospheric $\Delta^{14}C$ during the last 50 kyr, *Earth Planet. Sci. Lett.*, *200*, 179–192.

Mazaud, A., M. A. Sicre, U. Ezat, J. J. Pichon, J. Duprat, C. Laj, C. Kissel, L. Beaufort, E. Michel, and J. L. Turon (2002), Geomagnetic-assisted stratigraphy and sea-surface temperature changes in core MD94–103 (southern Indian Ocean): Possible implications for north-south climatic relationship around H4, *Earth Planet. Sci. Lett.*, *201*, 159–170.

Ninnemann, U. S., C. D. Charles, and D. A. Hodell (1999), Origin of global millennial scale climate events: Constraints from the Southern Ocean deep sea sedimentary record, in *Mechanisms of Global Climate Change at Millennial Time Scales*, *Geophys. Monogr. Ser.*, vol. 112, edited by P. U. Clark, R. S. Webb, and L. D. Keigwin, pp. 99–112, AGU, Washington, D. C.

Pahnke, K., and R. Zahn (2005), Southern Hemisphere water mass conversion linked with North Atlantic Climate variability, *Science*, *307*, 1741–1744.

Rintoul, S. R., C. W. Hughes, and D. Olbers (2001), The Antarctic Circumpolar Current system, in *Ocean Circulation and Climate*, edited by G. Siedler, J. Church, and J. Gould, pp. 271–302, Elsevier, New York.

Shackleton, N., M. A. Hall, and E. Vincent (2000), Phase relationship between millennial-scale events 64,000–24,000 years ago, *Paleoceanography*, *15*, 565–569.

Sicre, M. A., L. Labeyrie, U. Ezat, J. Duprat, J. L. Turon, S. Schmidt, E. Michel, and A. Mazaud (2005), Mid-latitude southern Indian Ocean response to Northern Hemisphere Heinrich events, *Earth Planet. Sci. Lett.*, *240*, 724–731.

Siddal, M., E. J. Rohling, A. Almogi-labin, C. Hemlebem, D. Meischner, I. Schmelzer, and D. A. Smeed (2003), Sea level fluctuations during the last glacial cycle, *Nature*, *423*, 853–858.

Stocker, T. F. (1998), The see-saw effect, *Science*, *282*, 61–62.

Stocker, T. F. (2002), North-south connections, *Science*, *297*, 1814–1815.

Stocker, T. F., and S. J. Johnsen (2003), A minimum thermodynamic model for the bipolar seesaw, *Paleoceanography*, *18*(4), 1087, doi:10.1029/2003PA000920.

Tauxe, L., J. L. La Brecque, R. Dodson, M. Fuller, and J. Dematteo (1983), "U" channels: A new technique for paleomagnetic analysis of hydraulic piston cores, *Eos Trans. AGU*, *64*, 2–19.

Thompson, R., and F. Oldfield (1986), *Environmental Magnetism*, 227 pp., Allen and Unwin, St. Leonards, N. S. W., Australia.

Verosub, K. L., and A. P. Roberts (1995), Environmental magnetism: Past, present, and future, *J. Geophys. Res.*, *100*, 2175–2192.

Weeks, R. J., C. Laj, L. Endignoux, M. Fuller, A. P. Roberts, R. Manganne, E. Blanchard, and W. Goree (1993), Improvements in long-core measurements techniques: Applications in paleomagnetism and palaeoceanography, *Geophys. J. Int.*, *114*, 651–662.